Nano Research

Open Access

Research Article

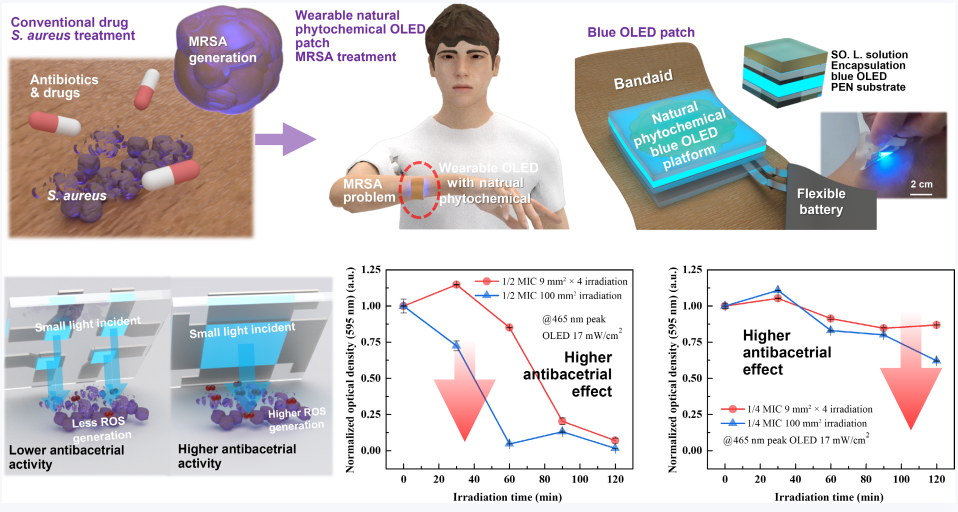
Wearable blue OLED patch using natural antibacterial phytochemicals for non-antibiotic treatment against *Staphylococcus aureus*

Young Woo Kim[1,§], Jae-Young Jeong[2,§], Eou-Sik Cho[3], Sang Jik Kwon[3], Jeong Hyun Kwon[4] ✉, You-Jin Hwang[5] ✉, and Yongmin Jeon[6] ✉

[1] *Department of Semiconductor Engineering, Gachon University, Seongnam 13120, Republic of Korea*
[2] *Department of Biohealth & Medical Engineering, Gachon University, Seongnam 13120, Republic of Korea*
[3] *Department of Electronics Engineering, Gachon University, Seongnam 13120, Republic of Korea*
[4] *School of Semiconductor Engineering, Chungbuk National University, Cheongju 28644, Republic of Korea*
[5] *Department of Biomedical Engineering, Gachon University, Seongnam 13120, Republic of Korea*
[6] *Department of Information Display, Kyung Hee University, Seoul 02447, Republic of Korea*
§ *Young Woo Kim and Jae-Young Jeong contributed equally to this work.*

Cite this article: *Nano Research*, **2025**, *18*, 94907409. https://doi.org/10.26599/NR.2025.94907409

ABSTRACT: Currently, there is growing interest in non-antibiotic treatments due to the emergence of multidrug-resistant bacteria. Moreover, photodynamic therapy is advantageous as it is non-invasive and does not lead to resistance development. Unlike traditional light therapy platforms, such as light amplification by stimulated emission of radiations (LASERs) and light-emitting diodes (LEDs), organic LEDs (OLEDs) are lightweight, flexible, and compact, enabling real-time treatment in everyday life. Additionally, as a surface-emitting light source, OLEDs deliver a uniform treatment effect over a large area. In this study, we explored the synergistic effect on *Staphylococcus aureus* (*S. aureus*) using a natural non-antibiotic material, *Sanguisorba officinalis* L. extract solution (SO. L.), and 465 nm peak patchable OLEDs depending on both irradiation time and light source area at an intensity of 17 mW/cm². The results confirmed that antibacterial activity increased with light exposure to SO. L., and further increased as the area of the surface light source expanded. Moreover, the effect was noted with another natural non-antibiotic material. This study validated the non-antibiotic treatment using antibacterial synergistic activity between natural antibacterial phytochemicals and OLEDs and its free-standing antibacterial activity against antibiotic resistance in *S. aureus*.



KEYWORDS: organic light-emitting diodes (OLEDs), antibacterial, reactive oxygen species (ROS), natural phytochemical, *Staphylococcus aureus* (*S. aureus*)

Received: January 9, 2025; **Revised:** March 5, 2025; **Accepted:** March 28, 2025

✉Address correspondence to Yongmin Jeon, yongmin@khu.ac.kr; You-Jin Hwang, gene@gachon.ac.kr; Jeong Hyun Kwon, love6539@cbnu.ac.kr

1 Introduction

Since the introduction of penicillin, the mortality rate from bacterial skin tissue infections caused by *Staphylococcus aureus* (*S. aureus*) has significantly decreased [1]. These antibiotics have saved countless lives by treating various bacterial infections [2, 3]. However, infections caused by *S. aureus* remain the most prevalent and lethal pathogens [4, 5]. *S. aureus* exacerbates skin diseases by producing toxins during infection, leading to conditions, such as furuncles, impetigo, folliculitis, abscesses, furunculosis, hidradenitis suppurativa, and mastitis [4–6]. However, treatment of *S. aureus* with antibiotics can lead to methicillin-resistant *S. aureus* (MRSA), complicating the treatment [7–9]. Multidrug-resistant (MDR) organisms pose significant challenges even when antibiotics are administered promptly after an injury [10].

Non-antibiotic treatments based on natural phytochemicals and light-based antimicrobial treatments are known to overcome antibiotic resistance in *S. aureus* and MDR microorganisms [11, 12]. These treatments exhibit significant antibacterial activity against MDR microorganisms. Additionally, natural phytochemical methods are regarded as attractive and environmentally friendly due to their low cost, non-polluting nature, availability, and reduced risk of developing antibiotic resistance [11–14]. Various studies have confirmed the antimicrobial activity of naturally occurring flora against *S. aureus, Bacillus subtilis, Bacillus thuringiensis, Pseudomonas lachrymans, Agrobacterium tumefaciens, Xanthomonas vesicatoria*, and *Ralstonia solanacearum* [15, 16]. Currently, oregano oil is extensively utilized in cosmetics, food preservatives, and additives [11, 12]. These natural phytochemical-based drugs contain flavonoids, polyphenols, and polysaccharides, which exhibit antibacterial, antioxidant, anticancer, and anti-inflammatory properties [14, 17–20].

This antibacterial activity effect can also be confirmed in antibacterial photodynamic therapy (PDT). Bacteria, such as *S. aureus* and *Escherichia coli* (*E. coli*), exhibit antibacterial activity when exposed to ultraviolet C (UVC) [21, 22]. However, because UVC rays can also damage human cells, using them directly on humans is not compatible [23–25]. Consequently, research into antibacterial activity using the blue light spectrum, which avoids UVC rays, is ongoing, but this method requires high outputs to achieve antibacterial effects and might still harm host cells. Additionally, a method involves activating cellular transcription factors by generating reactive oxygen species (ROS) with the aid of a photosensitizer (PS) and light in the visible spectrum [26–30]. This technique minimizes the toxicity to humans while selectively targeting bacteria and cancer cells.

The method of treating infectious diseases and wounds with light sources offers several advantages over drug treatments, including being non-invasive, effective, and resistance-free. Various light-based treatments, such as photobiomodulation (PBM) and PDT with PS, are available. PBM activates cytochrome c oxidase (CCO) by irradiating cells with light to enhance the rate of cell proliferation [31–34]. Traditionally, PDT has been administered using light amplification by stimulated emission of radiations (LASERs) and light-emitting diodes (LEDs) [35–37]. However, recent advances in wearable organic LEDs (OLEDs) have led to the proposal of a light therapy platform capable of providing real-time treatment in daily life. Additionally, OLEDs are highly flexible, can be freely deposited on any shaped substrate, and are lightweight [31, 32]. These properties enable the versatile use of OLEDs on various substrates, including polyethylene terephthalate (PET), paper, fiber, and fabric [32, 38–40].

There are numerous prior studies on the anti-bacterial and anti-cancer effects of OLEDs, quantum dots LEDs (QLEDs), and micro LEDs (μ-LEDs). Initially, research involving OLEDs addressed cancer cells and bacteria treatment using PSs, such as BODIPY, 5-aminolevulinic acid (ALA), and methylene blue [27, 31, 41]. QLED studies were performed at a low intensity (1.8 mW/cm^2), and anticancer research involved PSs, such as ALA, photofrin, and talaporfin [42, 43]. Moreover, research using μ-LEDs focused on anticancer and antibacterial experiments with PSs, such as fotoditazin and verteprofin [44, 45]. All these studies utilized synthetic PSs instead of natural phytochemicals (as shown in Table 1).

In PDT using PSs from established antibacterial and anticancer drugs, there can be adverse effects on the human body depending on the type of PS used, and controlling the dosage of the PS and light output is challenging [46]. Furthermore, antibacterial treatments using only light frequently pose risks of human cell damage through UVC and require high-output light even within the visible range, complicating the mitigation of human cell damage. However, using natural products as PSs leads to fewer side effects on the human body compared with traditional PSs, allowing for adjustable drug or light dosage as needed. Additionally, using OLEDs enables uniform light irradiation over the affected area

Table 1 Comparison of various platforms against anti-bacterial, anti-cancer, and PDT

Platform	Peak wavelength (nm)	Irradiation intensity	Type of drug	Substance (chemical)	Target	Device characteristics	References
OLED	465	17 mW/cm^2	SO. L.	Natural	*S. aureus* (bacteria)	Flexible, wearable	This work
LED	465, 520, 590, and 625	93 mW/cm^2@465 nm	SO. L.	Natural	*S. aureus* (bacteria)	Rigid, point light	Previous work [47]
OLED	660	35 mW/cm^2	BODIPY	Artificial (PS)	Melanoma (cancer)	Flexible, wearable	[31]
OLED	635	3 mW/cm^2	ALA	Artificial (PS)	Glioma (cancer)	Flexible, wearable	[41]
OLED	610	5 mW/cm^2	Methylene blue	Artificial (PS)	*S. aureus* (bacteria)	Flexible, wearable	[27]
QLED	623	1.8 mW/cm^2	ALA	Artificial (PS)	Carcinoma (cancer)	Flexible, wearable	[42]
QLED LED	630 and 635 (QLED), 665 (LED)	1.8 mW/cm^2@QLED, 130 mW/cm^2@LED	Photofrin, ALA, talaporfin	Artificial (PS)	A431 (cancer)	Flexible, wearable	[43]
μ-LED	650	2 mW/cm^2	Fotoditazin	Artificial (PS and photodithazine)	*Cutibacterium acnes* (bacteria)	Rigid	[44]
μ-LED	690	0.15, 7.5, 25, and 50 mW/cm^2	Verteporfin	Artificial (PS)	CT26 (cancer)	Flexible, implantable	[45]

because it employs a surface light source, enhancing the potential for application in wearable devices.

In a previous study using these light sources and natural phytochemical-based medicines, we observed significant antibacterial activity against *S. aureus* at lower medicine concentrations using LEDs and *Sanguisorba officinalis* L. (*S. officinalis* L.) ethyl alcohol extract (SO. L.) [47]. This confirmed the synergistic antibacterial effects of visible light range and natural phytochemicals against *S. aureus*. Adding a photoreactive natrual phytochemical antibacterial material also enabled antibacterial activity with low-output light sources, although it was challenging to determine the precise antibacterial conditions due to uneven light distribution from the point LED source.

Building on previous research, this study aims to present improved results using wearable OLEDs. This study builds upon previous research by addressing the limitations of using rigid LED light sources. In earlier studies, only the light synergy effect on SO. L. solution was confirmed using SO. L. and LED. However, these studies were constrained by the rigidity of the LED light source, which made it unsuitable for developing a wearable platform capable of providing continuous light therapy in daily life [47]. Therefore, this study focuses on developing a treatment platform for MDR microbial strains by leveraging the synergy between low-output blue light and natural extracts in a wearable blue OLED with a surface light source. We studied the synergistic effect of *S. aureus* exposure to wearable OLED at a wavelength of 465 nm in a SO. L. containing phytochemicals solution for increments of 0, 30, 60, 90, and 120 min at an intensity of 17 mW/cm^2. Consequently, we aimed to assess the synergy and conditions of antibacterial activity between the wearable blue OLED with surface light source and natural extracts and to evaluate how the antibacterial activity varies with different light source areas. Through this, the research investigated the effective treatment of MDR microbial strains using phytochemical-based medicine and explored life-time treatment options using wearable OLEDs to provide sustained resistance and continuous therapy.

2 Experimental

2.1 Fabrication of patchable blue OLED

Using a pre-deposited glass substrate (SJ Company, Korea) with indium tin oxide (ITO) 150 nm and a polyethlene naphthalate (PEN) substrate (AMG, Korea), all OLEDs were manufactured sequentially using thermal evaporation OLED deposition equipment: ITO 150 nm served as the anode, followed by molybdenum trioxide (MoO_3) 5 nm as the hole injection layer (HIL), N,N'-di(1-naphthyl)-N,N'-diphenyl-(1,1'-biphenyl)-4,4'-diamine (NPB) 40 nm for the hole transport layer (HTL), 2-methyl-9,10-di(2-naphthyl)anthracene:p-bis(p-N,N-di-phenyl-aminostyryl) 3 wt.% (MADN:DSA-Ph 3 wt.%) 25 nm as the emission layer (EML), bis(10-hydroxybenzo[h]quinolinato)-beryllium ($Bebq_2$) 10 nm for electron transfer layer (ETL), cesium carbonate (Cs_2CO_3) 1 nm as the electron injection layer (EIL), and aluminum (Al) 100 nm as the cathode.

Additionally, we used 10 μm PET with deposition of 100 nm of Al_2O_3 for the encapsulation of the manufactured blue OLED. Subsequently, the blue OLED was integrated and attached to a standard bandaid. To operate this blue OLED bandaid, a flexible battery was connected.

2.2 Device characterization

The optical and electrical properties of the patchable blue OLED were measured using a spectro-radiometer (CS-2000, Konica Minolta Inc.) and a source meter (Keithley 2401, Keithley Inc.), respectively. The lifetime reliability of the patchable blue OLED was assessed through constant current operation in the air (M6100, McScience Inc.). Additionally, the temperature of the patchable blue OLED was recorded with a Thermal Imaging Camera (HT-19, HTI). The bending reliability was evaluated by flexing the device on a 1 Axis Motion Controller (STM-1-TS, TS-ONE) and measuring it using a spectro-radiometer (CS-2000, Konica Minolta Inc.).

2.3 Manufacturing process of *S. officinalis* L. solution

S. officinalis L. solution was prepared using the same method as in the previous study [47]. *S. officinalis* L. used in this study was procured from Samhong Medicinal Herb Market (Seoul, Republic of Korea). *S. officinalis* L. was ground into a powder, then macerated in 70% ethyl alcohol at 110 rpm for 24 h. The ratio of *S. officinalis* L. powder to 70% ethyl alcohol was set at 1:10 (w/v). The supernatant of the extract was then separated, centrifuged at 3000 rpm for 10 min, and concentrated under reduced pressure at 50 °C using a rotary evaporator WEV-1001V (Daihan Scientific Co., Wonju, Republic of Korea). The resulting concentrate was dried and redissolved at a concentration of 40 mg/mL in 10% dimethyl sulfoxide (DMSO; Sigma Chemical Co., St. Louis, MO, USA) aqueous solution, then filtered through Whatman filter paper No. 2 (Whatman, Kent, UK). The solution was subsequently sealed in conical tubes and stored at 4 °C until further use.

2.4 Absorbance measurement of *S. officinalis* L. solution

The absorbance peak measurement was conducted to analyze the optical properties of antibacterial ingredients present in the *S. officinalis* L. solution [47]. The solution was diluted to various concentrations (0.25, 0.5, 1, 2, and 4 mg/mL) using 10% DMSO aqueous solution and dispensed at 200 μL into 96 well plates. Absorbance peaks were recorded at 2 nm intervals from 300 to 800 nm using a multimode plate reader (Tecan, Infinite™ M200 PRO, Männedorf, Switzerland).

2.5 Measurement of total content of major ingredient in SO. L. solution

Measurements of total content for various ingredients were conducted to identify the antibacterial active compounds in the SO. L. solution. Assays conducted included 2,2-diphenyl-1-picrylhydrazyl (DPPH), total sugar content (TSC), total flavonoid content (TFC), and total polyphenol content (TPC). The TSC was determined using the phenol-sulfuric acid method by Dubois et al. [48]. The procedure involved mixing 0.6 mL of sample with 0.3 mL of 5% phenol solution in a test tube, adding 1.5 mL of concentrated sulfuric acid, stirring, and heating for 30 min at a constant temperature of 85 °C in a preheated water bath, followed by cooling for 10 min. Afterward, 200 μL of the sample solution from a 96 well-plate was used for absorbance measurement at 490 nm using a multimode plate reader (Tecan, Infinite™ M200 PRO, Männedorf, Switzerland), with glucose (Sigma-Aldrich) serving as a standard. A standard calibration curve was subsequently created for quantification. TFC was determined by mixing the solution with 1 N sodium hydroxide and diethylene glycol in a 1:1:10 ratio and reacting at 37 °C for 1 h [49]. Absorbance was measured at 420 nm

using the same multimode plate reader. The standard curve was prepared using quercetin, and flavonoid content was reported as milligrams of quercetin equivalent (mg QE) per gram of sample. TPC was measured by diluting a 2 N Folin–Ciocalteau solution 1/10 in deionized (DI) water with 100 μL of solution and adding 500 μL, followed by a 4 min wait and a 400 μL addition of sodium carbonate (75 g/L) [50]. After reacting for 2 h, absorbance was measured at 765 nm using the multimode plate reader. The standard curve was prepared using gallic acid, and phenolic content was expressed as mg gallic acid equivalent (GAE). The DPPH assay was conducted using the OxiTec™ DPPH Antioxidant Assay Kit (biomax, Guri, Republic of Korea), mixing the solution, assay buffer, and DPPH solution in a 1:4:5 ratio and reacting for 30 min at room temperature in a shaded area. Absorbance was measured at 517 nm, a standard curve was prepared using Trolox, and the Trolox equivalent antioxidant capacity (TEAC) was calculated using the following equation and expressed as a percentage

$$\text{TEAC} = \text{IC50 of sample}/\text{IC50 of Trolox} \times 100 \quad (1)$$

where IC50 represents the concentration required to inhibit free radicals by 50% through antioxidant activity.

2.6 Bacterial culture

Bacterial culture was performed using the same method as in previous studies [47]. *S. aureus* (ATCC 29213) utilized in this experiment was obtained from the American Type Culture Collection (ATCC; Manassas, VA, USA). This strain was preserved at −80 °C with 20% glycerol (v/v) and used only after subculturing on a brain heart infusion (BHI; Kisan Bio, Seoul, Republic of Korea) agar at 37 °C for 24 h. Before experimentation, colonies were isolated from subcultured agar and cultured in BHI broth at 37 °C for 24 h, with agitation at 120 rpm. Subcultures were performed biweekly to ensure bacterial viability.

2.7 Measuring antibacterial activity synergy effect with *S. officinalis* L. solution and blue OLED against MRSA

Minimum inhibitory concentration (MIC) was assessed to evaluate the synergistic antibacterial effects between SO. L. solution and blue OLED against *S. aureus*. MIC determination involved a minor adaptation of the broth microdilution method from a previous study [47]. Briefly, 200 μL of the sample was inoculated into the first well of a 96-well plate and sequentially diluted by half down to 1/4 of the previously measured MIC [51]. *S. aureus* was then diluted to 1×10^6 CFU/mL (CFU stands for colony-forming unit) in BHI broth and added to each well in 100 μL aliquots to reach a total of 200 μL. Irradiation was applied using a blue OLED producing 17 mW/cm^2 at 30 min intervals up to 120 min, followed by incubation with agitation at 110 rpm at 37 °C for 24 h. Absorbance was measured at 595 nm using a spectrophotometer (Multiskan FC; Thermo Fisher Scientific, Waltham, MA, USA). The assessment of antibacterial activity was based on the half-maximal inhibitory concentration (IC50) of *S. aureus*.

3 Results and discussion

3.1 Concept of patchable blue OLED applied natural phytochemical antibacterial

Phototherapy platforms utilizing LASER or LED are constrained by their equipment size, limiting both duration and area of application, making it challenging to achieve uniform treatment across extensive areas, such as widespread skin infections or wounds. A previous study on antibacterial effects against *S. aureus* utilized SO. L. solution coupled with blue LED visible light [47]. When applied to the human body, similar limitations are expected. This study employed blue OLEDs, which can be adhered to human skin, to address these limitations.

Historically, *S. aureus* has been managed using antibiotic drug therapy, which bears the risk of causing or exacerbating MRSA, diminishing the treatment's effectiveness. Additionally, UV lamps have been used for sterilizing *S. aureus* on surfaces like food and skin; however, the intense energy of UV light can damage the skin. To mitigate these problems, we presented a novel platform for MRSA treatment that involves a wearable blue OLED patch infused with natural phytochemicals designed for direct skin application, as demonstrated in Fig. 1(a).

First, we prepared the SO. L., which we dried completely, including the stems, leaves, and roots, and then ground into a fine powder. We then created the SO. L. mixture by combining the finely ground powder with 70% ethyl alcohol, maintaining a material powder-to-solvent ratio of 1:10 (w/v). The supernatant is separated and concentrated through centrifugation, as illustrated in Fig. 1(b). The resulting SO. L. solution is a crude extract that has not yet undergone component fractionation. Consequently, various phenolic compounds, polysaccharides, and flavonoids within the SO. L. solution contributes to its antibacterial activity [14, 17–20]. A schematic diagram depicting the antibacterial activity of *S. aureus*, a pathogen that infects human skin and causes various skin infections, illustrates the application of a flexible blue OLED patch in combination with the SO. L. solution in Fig. 1(c). *S. aureus* harbored in the skin is inactivated by damage to cells and the activation of transcription factors caused by ROS produced by various antibacterial agents in the SO. L. solution when exposed to blue OLED light [52] (Fig. 1(d)). Wearable blue OLED patches utilizing flexible substrates are applied to various materials, such as paper, PET, PEN, and fabric [32, 38–40], as shown in Fig. 1(e). In this study, the blue OLED patches were manufactured by affixing a bandaid and a flexible battery to the blue OLED, which was previously deposited on a PEN substrate coated with ITO. Additionally, the SO. L. solution is applied to the platform, with operating images visible in the photo in Fig. 1(f). The production and operation of the blue OLED patches are also depicted in Video S1 in the ESM.

3.2 Manufacturing process and characteristics of SO. L. solution and patchable blue OLED

Prior to the antibacterial activity test, the production of each SO. L. solution and OLED were analyzed. As depicted in Fig. 1 above, the dried SO. L. was ground into a powder and then dissolved in 70% ethyl alcohol to concentrate it, as illustrated in Fig. 2(a).

A patchable blue OLED was produced by depositing OLED materials through a thermal evaporation process onto a PEN substrate (AMG, Korea), where ITO was pre-deposited. On both the PEN substrate and glass ITO, layers of MoO_3, NPB, MADN:DSA-Ph 3 wt.%, $Bebq_2$, Cs_2CO_3, and lastly, Al as a cathode were sequentially deposited, as illustrated in Fig. 2(b). Consequently, we fabricated an OLED with an emitting area of 100 mm^2 and another with 9 mm^2 that both emit blue light.

Upon application of the patch on MRSA-infected skin, the

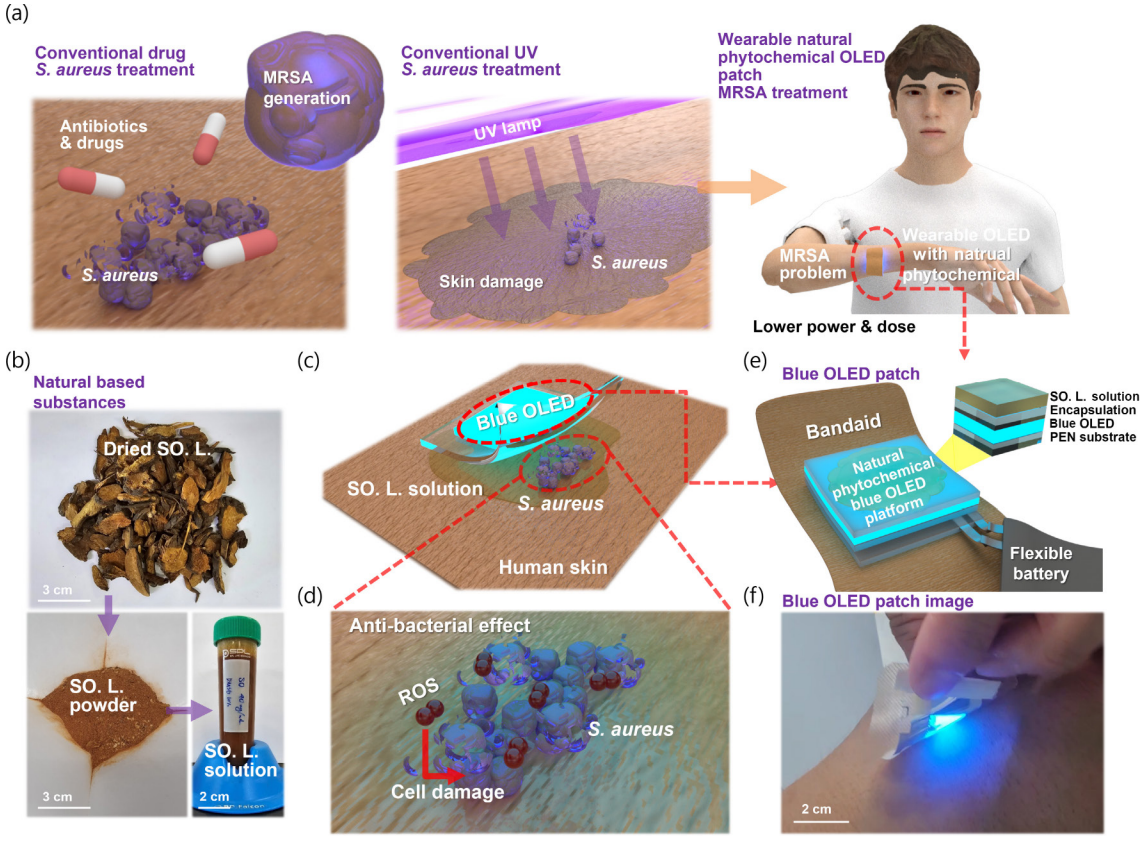


Figure 1 Concept of natural phytochemical and patchable blue OLED based antibacterial effect. (a) Schematic illustration of the MRSA treatment evaluation. (b) Photo of natural-based substances formulated as an antibacterial solution. (c) Schematic illustration of the antibacterial effect of a blue OLED patch and SO. L. solution against *S. aureus*. (d) Schematic illustration of ROS generation in *S. aureus* using this platform. (e) Schematic structure of the patchable blue OLED platform. (f) Photo of the patchable blue OLED platform.

following structure emerges. A SO. L. solution was applied to the MRSA-infected skin, and a blue OLED was positioned over it. This OLED was integrated into the bandaid and powered by a flexible battery, as depicted in Fig. 2(c).

The prepared solution was divided into concentrations of 0.25, 0.5, 1.0, 2.0, and 4.0 mg/mL, and the absorbance was measured at a temperature of 37.2 °C (Fig. 2(d)). As the concentration increased, the absorbance of light increased, resulting in higher absorption peaks at shorter wavelengths. Furthermore, an absorption peak was observed in the 360 nm range; when irradiated with light of this wavelength, the antibacterial activity efficiency may surpass that of other wavelengths. At 465 nm, a low absorption peak was observed in this study. However, upon extending the wavelength range into the visible spectrum, a relatively high absorption rate was detected compared to other wavelength regions, as shown in Fig. S1 in the Electronic Supplementary Material (ESM). Previous studies have also demonstrated antibacterial synergy in the visible light region despite its typically lower absorption levels [47]. Based on these findings, SO. L. solution was employed as a natural antibacterial phytochemical in this experiment. The total content of polyphenols, flavonoids, and sugars, known to exhibit antioxidant and antibacterial activities, was quantified to determine the class of compounds contributing to the antibacterial activity in the SO. L. solution (Table 2). Measurements of antioxidant activity and the total content of each class of compounds were taken using known standard substances. The measurements revealed the following results: Antioxidant activity was 74.40553% ± 4.997551%, TSC was 23.20606 ± 0.483644 glucose equivalent (GE) μg/100 μg. TFC was determined by mixing the solution with 1 N sodium hydroxide and diethylene glycol in a 1:1:10 ratio and reacting at 37 °C for 1 h [49]. Absorbance was measured at 420 nm using the same multimode plate reader. The standard curve was prepared using quercetin, and flavonoid content was reported as mg QE per gram of sample. TPC was measured by diluting a 2 N Folin–Ciocalteau solution 1/10 in DI water with 100 μL of solution and adding 500 μL, followed by a 4 min wait and a 400 μL addition of sodium carbonate (75 g/L) [50]. TFC was 40.16667 ± 9.024655 QE μg/100 μg, and TPC was 43.94667 ± 0.718424 GE μg/100 μg. The antioxidant activity measured over 70% higher than the standard material. A comparative analysis of the total content in each series confirmed that flavonoid and polyphenol levels were higher than sugar content. Given their robust antibacterial and antioxidant properties, flavonoids and polyphenols are expected to be the primary components exhibiting antibacterial activity in SO. L. solutions. This led to a focused investigation of flavonoid and polyphenol components with antibacterial activity in *S. officinalis* L. used in the experiment (Table S1 and Fig. S2 in the ESM). The well-known

Table 2 Total content of major antibacterial compounds in SO. L. and U. G.

Extracts	TEAC (%)	TSC (GE μg/100 μg)	TFC (QE μg/100 μg)	TPC (GAE μg/100 μg)
SO. L. crude	74.40553 ± 4.997551	23.20606 ± 0.483644	40.16667 ± 9.024655	43.94667 ± 0.718424
U. G. crude	72.97366 ± 7.3544	23.21212 ± 1.311782	69.38889 ± 8.505441	65.93333 ± 0.815435

antibacterial active components of *S. officinalis* L., such as catechin, gallic acid, quercetin, and sanguiin H-6, are listed with their molecular characteristics in the following table (Table S1 and Figs. S2 and S3 in the ESM) [53–55]. Catechin is known to exhibit antibacterial activity against bacterial cells by increasing ROS and decreasing antioxidant enzymes, such as superoxide dismutase (SOD) and catalase, thereby inducing oxidative stress [56–60]. Gallic acid exhibits antibacterial activity against various strains alone, and its activity increases when combined with antibiotics [61–64]. Quercetin produces antibacterial effects through the decomposition of bacterial cell walls and membranes, nucleic acid synthesis, inhibition of biofilm formation, and reduced expression of virulence factors [65, 66]. Sanguiin H-6 exhibits antibacterial activity against various strains, even when used individually [67, 68]. Furthermore, these phenolic compounds serve as natural PSs in antibacterial PDT. Examples of such natural PSs include curcumin, hypericin, quercetin, hypocrellins A and B, resveratrol, gallic acid, aloe emodin, celastrol, and riboflavin, each possessing various biological properties [69, 70]. In antibacterial PDT, the PS generates ROS when irradiated with the proper wavelength. It is divided into types 1 and 2 based on the photochemical reaction. In type 1 reactions, the PS, excited by light, transfers high-energy electrons to nearby molecules or molecular oxygen, creating ROS, such as hydrogen peroxide, superoxide anion, and hydroxyl radical. Type 2 involves the generation of highly reactive singlet oxygen by transferring energy from the PS to oxygen [69–73]. This photochemical reaction results in cell damage through oxidative stress that specifically targets bacterial cells, leading to antibacterial activity. It is influenced by particular substrates, PSs, and oxygen levels [69].

The manufactured OLED's emission spectrum is shown in Fig. 2(e), exhibiting peak irradiation at 465 nm, regardless of whether the substrate is composed of glass, PEN, or has a varying emission area.

The fabricated wearable blue OLED patch possesses a structure illustrated in Fig. 3(a). A flexible blue OLED was mounted on the bandaid and connected to a flexible battery. Furthermore, a SO. L. solution was applied on top of it. The blue OLED, at this stage, exhibits an energy band diagram as depicted in Fig. 3(b), thereby emitting light in the blue light region.

The physical characteristics of the devices were verified prior to confirming the antibacterial effect using the fabricated glass substrate OLEDs (100 and 9 mm^2) and PEN substrate OLED (100 mm^2). Figure 3(c) presents data that measure irradiance up to 17 mW/cm^2 for each device. At this time, OLED devices with a glass substrate recorded an irradiance of 17 mW/cm^2 at 8.5 V for a device area of 100 mm^2, and devices with an area of 9 mm^2 reached the same irradiance at 8.0 V. Moreover, devices using a PEN

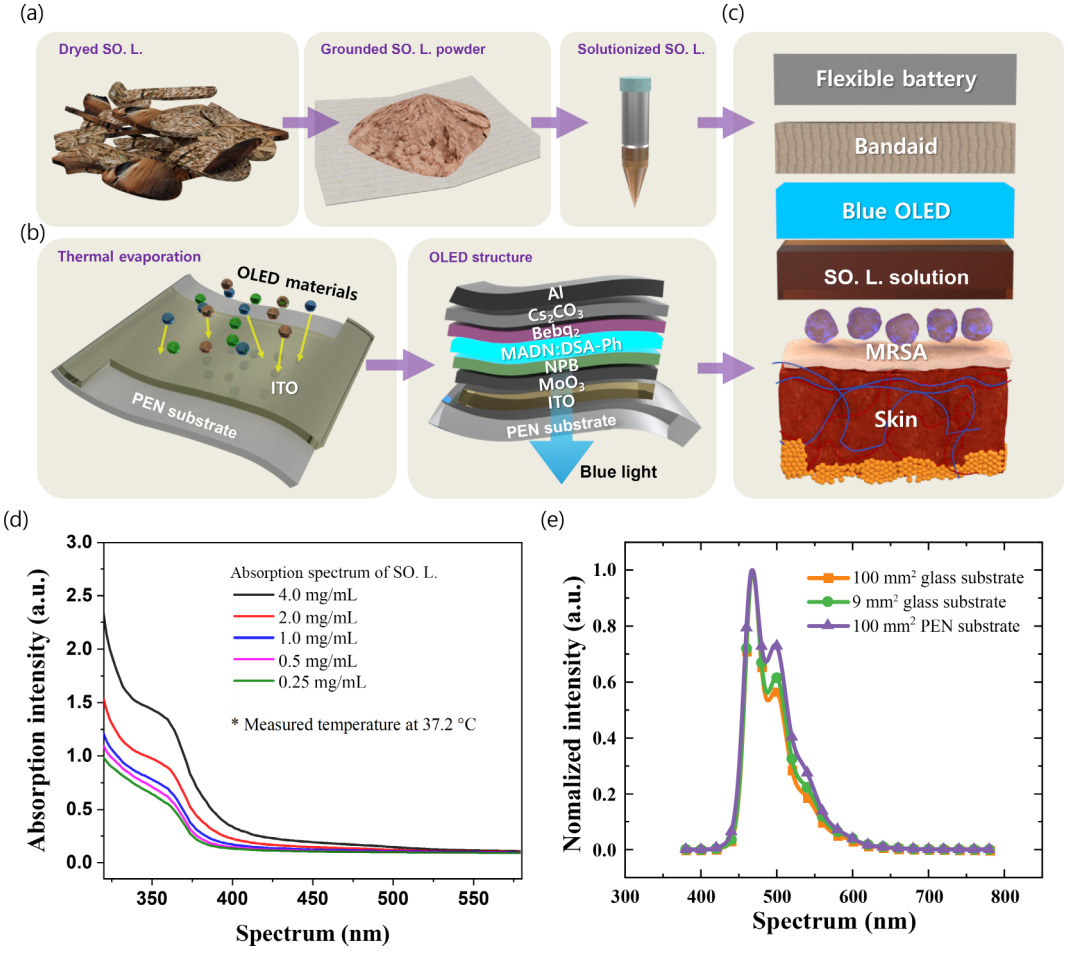


Figure 2 Manufacturing process and spectral characteristics of SO. L. solution and blue OLED. (a) Schematic illustration of the process to create solutionized SO. L. from natural substances. (b) Schematic illustration of blue OLED fabrication. (c) Schematic illustration of a wearable blue OLED patch applying natural phytochemical to MRSA-infected human skin. (d) Absorption intensity vs. spectrum graph of various concentrations of SO. L. solution. (e) Spectra graph of various substrates and areas of blue OLEDs.

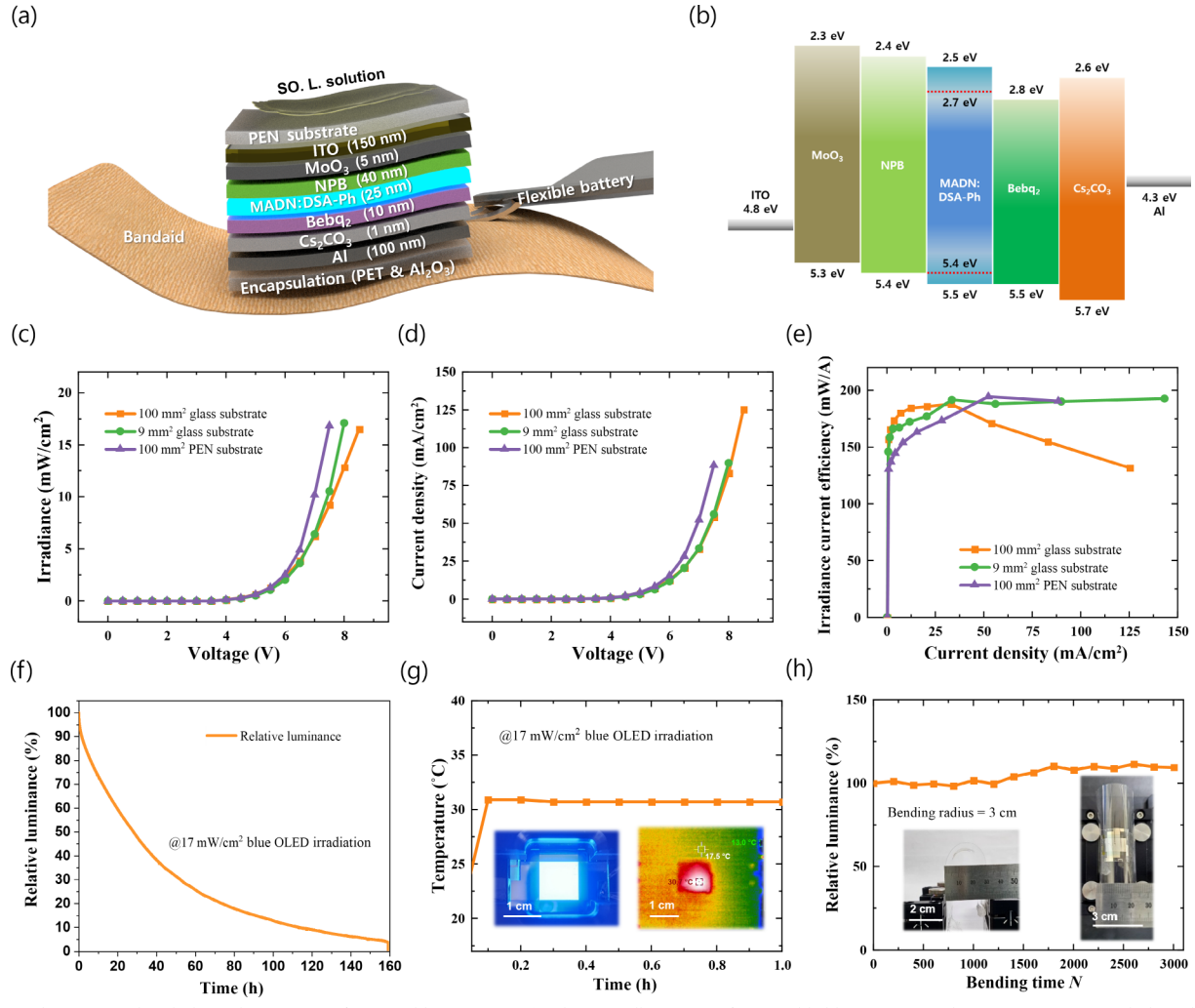


Figure 3 Electro-optical and physical properties of various blue OLEDs. (a) Schematic illustration of a wearable blue OLED patch incorporating natural phytochemical. (b) Energy band diagram of a wearable blue OLED patch. (c) Irradiance vs. voltage characteristics. (d) Current density vs. voltage characteristics. (e) Irradiance current efficiency vs. current density characteristics. (f) Lifetime reliability of blue OLED. (g) Driving temperature of blue OLED. (h) Bending reliability of blue OLED.

substrate with an area of 100 mm² achieved 17 mW/cm² at 7.5 V. The luminance characteristics for each device were approximately 12,000 cd/m², as illustrated in Fig. S4(a) in the ESM. At this stage, the surface resistance of each substrate was measured using a 4-point probe method, and the results were compared. As shown in Table S2 in the ESM, the device fabricated on the glass substrate (SJ Company, Korea) exhibited a surface resistance of 19.11 ± 2.40 Ω/sq, while the device using the PEN substrate (AMG, Korea) demonstrated a slightly lower surface resistance of 17.32 ± 1.13 Ω/sq. These measurements provide valuable insights into the electrical properties of the substrates used in this study. Additionally, the current injection characteristics were confirmed. At an irradiance of 17 mW/cm², the glass substrate with a 100 mm² emission area exhibited 125.21 mA/cm² at 8.5 V, the glass substrate with a 9 mm² emission area showed 89.95 mA/cm² at 8 V, and the PEN substrate with a 100 mm² emission area displayed 88.42 mA/cm²; these values confirm higher current injection characteristics at marginally lower voltages for the PEN substrate compared to the glass substrate, as detailed in Fig. 3(d). This difference is attributed to the slightly lower sheet resistance of the ITO electrode deposited on the PEN substrate compared to that on the glass substrate. Additionally, the irradiance current efficiency at an irradiance of 17 mW/cm² was measured as 131.72 mW/A for the 100 mm² glass substrate, 192.73 mW/A for the 9 mm² glass substrate, and 190.56 mW/A for the 100 mm² PEN substrate, as shown in Fig. 3(e). Similarly, the luminescence current efficiency can also be observed in Fig. S4(b) in the ESM.

The reliability of the PEN substrate OLED with an emitting area of 100 mm² is demonstrated by the following figures. In Fig. 3(f), the device was driven for about 40 h at 17 mW/cm² until its luminescence intensity reached 50%, and it continued to emit light for approximately 160 h. Additionally, the device's temperature, measured during the 1 h operation, stabilized at around 31 °C and consistently remained below 43 °C, confirming its safety against low-temperature burns even when applied to skin [74] (Fig. 3(g)). Furthermore, to assess flexibility attributes, the brightness characteristics were tested up to 3000 cycles with a bending radius of 3 cm at a consistent driving current of 100 mA; the results confirmed that the brightness did not degrade over these cycles (Fig. 3(h)). The overall image of the patchable blue OLED, constructed using the PEN device, is displayed in Fig. S5 in the ESM.

3.3 Natural phytochemical antibacterial effect with different emit sizes of patchable blue OLED *in-vitro*

Synergy in antibacterial activity between patchable blue OLED and SO. L. solution, containing natural phytochemicals, was confirmed through MIC measurement in an *in-vitro* setting. Variations in the antibacterial efficacy related to the OLED area were also noted, as shown in Fig. S6 in the ESM. Additionally, post-irradiation, the results visibly exhibited distinct characteristics, as depicted in Fig. S7 in the ESM. This experiment was conducted under four distinct conditions: a control where only blue OLED was applied to *S. aureus*; a comparison condition where blue OLED was used in a 1 MIC setting, effectively eliminating all *S. aureus*; a scenario where blue OLED was used with SO. L. solution at half concentration; and an application involving blue OLED irradiation in a solution at 1/4 MIC concentration, as demonstrated in Fig. 4(a). Antibacterial activity was assessed based on the IC50 for *S. aureus* used in the experiment. Small-area OLEDs were directly irradiated with one well-plate per pixel (Fig. 4(b)). The energy densities delivered to cells by OLED were 30.6, 61.2, 91.8, and 122 J/cm^2 over durations ranging from 30 to 120 min, respectively. Small-area blue OLED demonstrated antibacterial activity beginning at 90 min at 17 mW/cm^2 at 1/2 MIC (91.8 J/cm^2 of energy density) when light was directed onto SO. L. solutions at varying concentrations, and no antibacterial activity was observed until 120 min at 1/4 MIC (Figs. 4(c)–4(g)). Additionally, the reduced light amount, according to the life of the device, was calculated to check whether the exact light dose was irradiated. When it was assumed that 17 mW/cm^2 of light was uniformly irradiated for 30–120 min was 100%, the light amount applied for 30–120 min was 98.6%–94.3% of the total light applied. The integrated area can be found in Fig. S8 in the ESM.

To verify the area-specific effect, large-area OLED experiments were conducted, as illustrated in Fig. 5(a). The irradiation energy densities were identical to those of small-area OLED, which are 30.6, 61.2, 91.8, and 122 J/cm^2 over durations of 30 to 120 min, respectively. Upon exposing the large-area blue OLED to SO. L. solutions at different concentrations, antibacterial activity was notably observed from 60 min at 17 mW/cm^2 at 1/2 MIC, with slight activity also detected from 60 min at 1/4 MIC (Figs. 5(b)–5(f)). This result, corroborated by data from Figs. 4 and 5, confirmed that irradiating with a certain amount of light through blue OLED enhances the antibacterial activity against *S. aureus* compared to using SO. L. solution alone. These results are succinctly presented in graphs as shown in Figs. S9(a) and S9(b) in the ESM.

Furthermore, compared to the experimental findings in Fig. 4, a

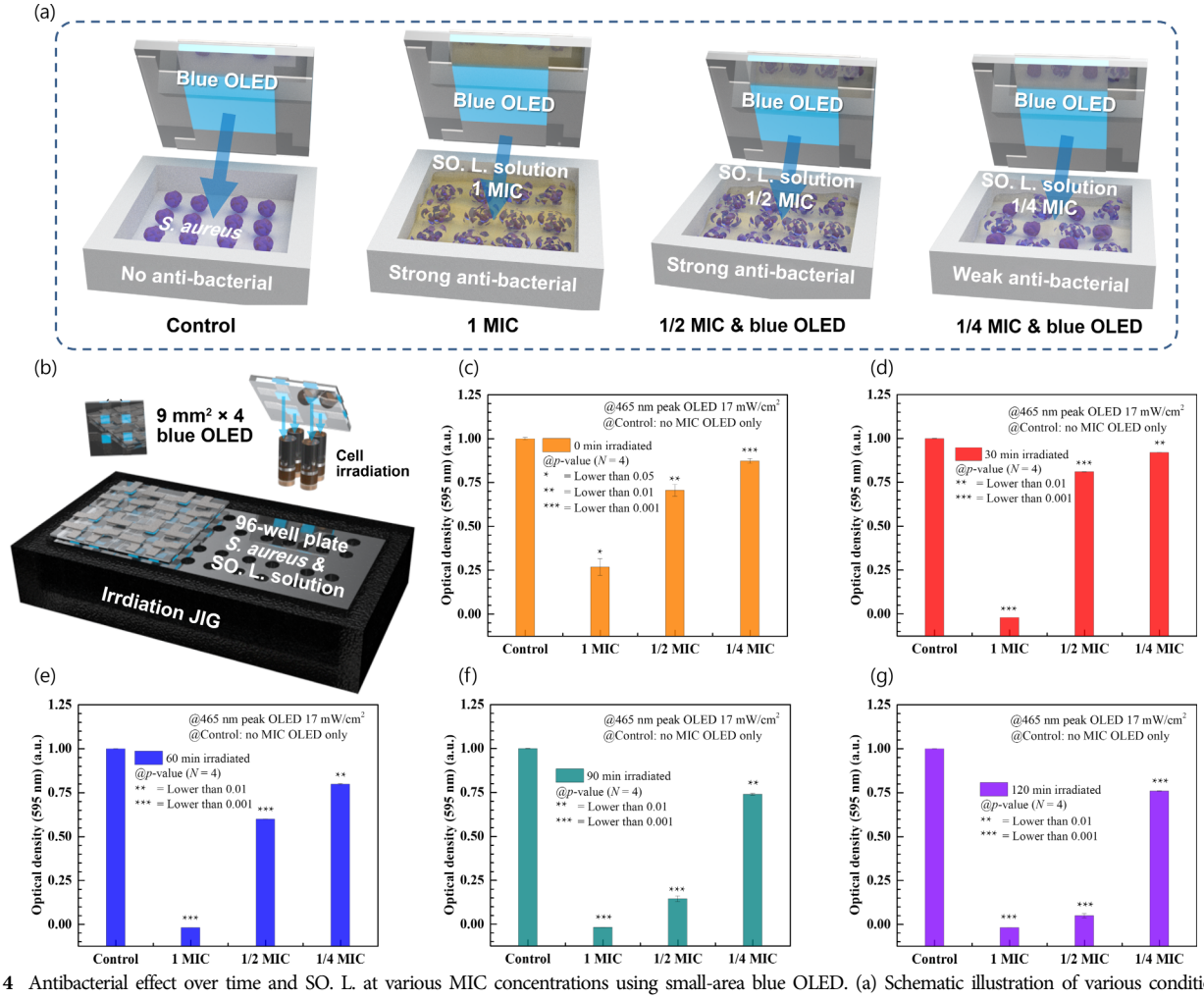


Figure 4 Antibacterial effect over time and SO. L. at various MIC concentrations using small-area blue OLED. (a) Schematic illustration of various conditions for *S. aureus* treatment using SO. L. and blue OLEDs. (b) Schematic illustration of irradiation against *S. aureus* with SO. L. solutions and small-area blue OLED. (c) *S. aureus* cell inhibition at 0 min of irradiation. (d) *S. aureus* cell inhibition at 30 min of irradiation. (e) *S. aureus* cell inhibition at 60 min of irradiation. (f) *S. aureus* cell inhibition at 90 min of irradiation. (g) *S. aureus* cell inhibition at 120 min of irradiation.

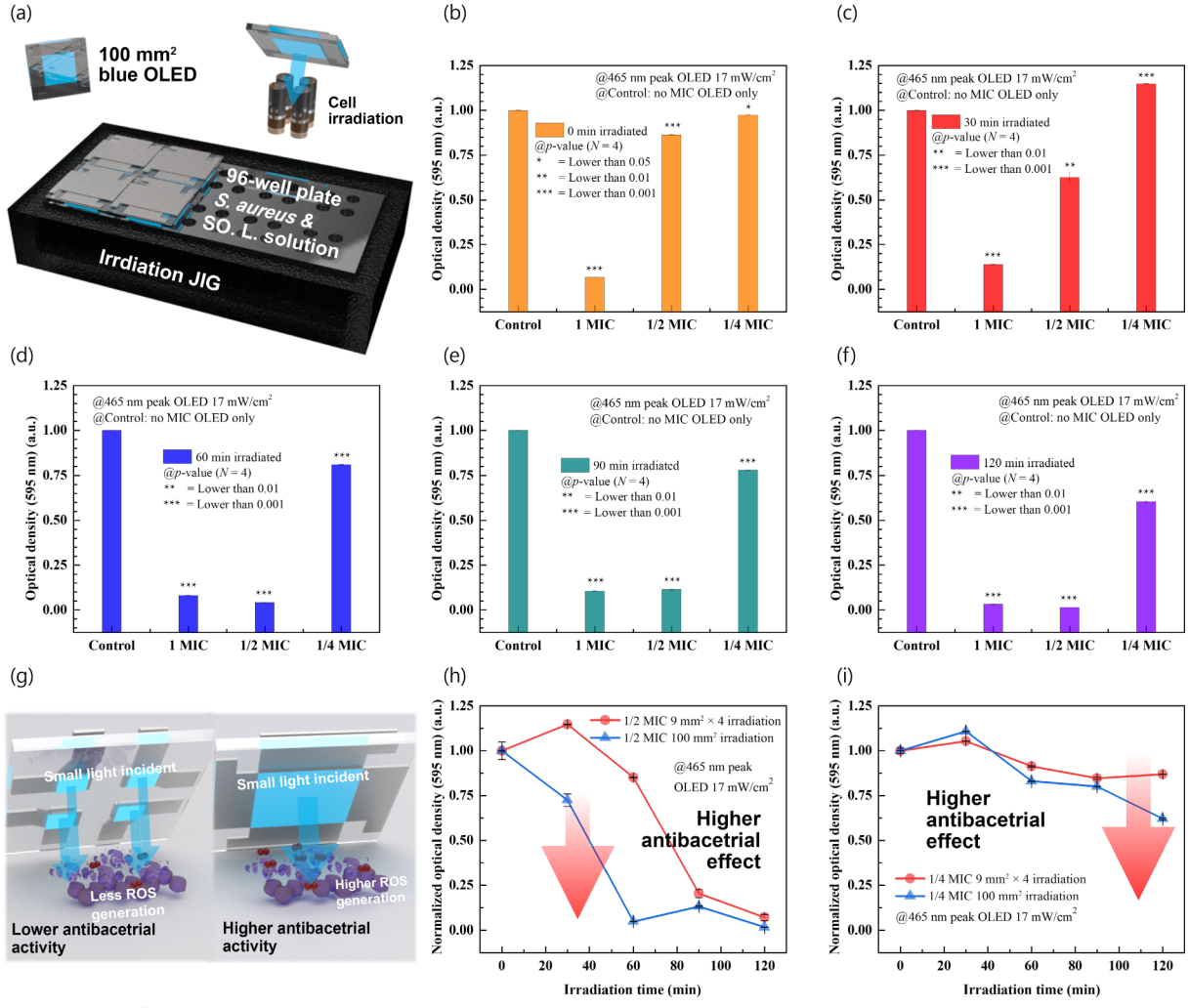


Figure 5 Antibacterial effect over time and SO. L. at various MIC concentrations using large-area blue OLED and comparison between OLED irradiation areas. (a) Schematic illustration of irradiation against *S. aureus* with SO. L. solutions and large-area blue OLED. (b) *S. aureus* cell inhibition at 0 min of irradiation. (c) *S. aureus* cell inhibition at 30 min of irradiation. (d) *S. aureus* cell inhibition at 60 min of irradiation. (e) *S. aureus* cell inhibition at 90 min of irradiation. (f) *S. aureus* cell inhibition at 120 min of irradiation. (g) Schematic illustration of antibacterial effects on various areas of OLEDs. (h) *S. aureus* cell inhibition in 1/2 MIC concentration of SO. L. solution with different irradiation areas of OLEDs. (i) *S. aureus* cell inhibition in 1/4 MIC concentration of SO. L. solution with different irradiation areas of OLEDs.

difference in antibacterial activity due to the light area was verified, as depicted in Fig. 5(g). When using small-area OLEDs, even with equivalent light intensity, the absolute amount of light reaching the target cells varies, influencing ROS generation. Accordingly, the area effects were substantiated by juxtaposing the results from experiments using both a small-area and a large-area blue OLED within a single graph. In Fig. 5(f), the SO. L. concentration at 1/2 MIC was normalized against the cell density at 0 min of irradiation. An analysis of the antibacterial effect by device area revealed a distinct effect starting from 60 min of irradiation in an OLED with an area of 100 mm². However, in devices with an area of 9 mm² × 4, antibacterial activity commenced from 90 min. Figure 5(i) is standardized based on cell density at 0 min irradiation time at a 1/4 MIC concentration of SO. L. Although the device with an area of 9 mm² × 4 did not exhibit significant antibacterial activity even after prolonged irradiation, it was observed that the device with an area of 100 mm² began to show antibacterial activity after 120 min. These findings indicate a synergistic effect of antibacterial activity arising from the variation in the absolute light amount.

Additionally, we tested the synergistic antibacterial effects of extract solutions on *Uncaria gambir* Roxb. (U. G.) and blue OLED. We conducted 30 min of irradiation ranging from 0 to 17 mW/cm² at concentrations of 1 MIC, 1/2 MIC, and 1/4 MIC of U. G. solution. The results demonstrated an antibacterial effect at 17 mW/cm² with an energy dose of 30.6 J/cm² at a 1/2 MIC concentration, as shown in Fig. S10 in the ESM.

In addition, the SO. L. solution may evaporate when dissolved in DI water. It was hypothesized that if moisture evaporates, the concentration of the solution could change, potentially altering the synergy effect of its antibacterial activity. To investigate this, a drying experiment was conducted using a 1 mL solution over a time period of 30–120 min, as suggested in this study. The results confirmed that approximately 20% evaporation occurred within 120 min, as shown in Fig. S11(a) in the ESM.

Furthermore, a study was performed to determine whether absorbance changes as the solution dries. The actual absorbance intensity was measured and confirmed, as illustrated in Figs. S11(b) and S11(c) in the ESM. The experimental results indicated no significant change in absorbance at approximately 20% evaporation. Although absorbance remains unchanged after drying, it is recommended to implement a wiping process after use to mitigate

potential side effects caused by the increased concentration of the solution.

4 Conclusions

In summary, we developed a life-compatible, patchable treatment platform for antibacterial activity, utilizing natural phytochemicals and patchable blue OLEDs. This platform can be applied directly to the human body and has been validated against *S. aureus*, showing effectiveness at low concentrations of natural phytochemicals. Moreover, we found that a surface light source offers more effective treatment than a point light source, and wide-area light sources are more effective than those with narrow areas.

Initially, *S. officinalis* L. *and* U. G. were finely ground and macerated in 70% ethyl alcohol to extract their active compounds by shaking extraction. After concentration and drying under reduced pressure, they were dissolved in a 10% DMSO aqueous solution to prepare a solution containing natural phytochemicals. These solutions displayed effective antibacterial activity against MRSA at a concentration of 1 MIC without any synergy with OLED.

Furthermore, we developed an OLED that performs similarly to or better than the reference OLED on a glass substrate in a patchable blue configuration. The glass substrate-based OLED achieved an irradiance of 17 mW/cm^2 at 8.5 V for the same emit area of the light source, while the flexible OLED based on a PEN substrate reached similar irradiance at 7.5 V. Additionally, irradiance current efficiency and current density were superior in the PEN substrate-based flexible OLEDs compared to those based on glass substrates. These flexible OLEDs have been integrated with conventional bandages and flexible batteries to lay the groundwork for their use as a flexible phototherapy platform.

Synergy effect of mixing natural phytochemicals and patchable OLED was confirmed. Based on the concentration of 1 MIC, where antibacterial activity is observed, the concentration was reduced to 1/2 and 1/4. The antibacterial activity was confirmed at these lower concentrations of MIC using OLEDs with emit areas of 9 and 100 mm^2. During this period, the blue OLED condition with an emitting area of 9 mm^2 displayed antibacterial activity with an energy dose of 91.8 J/cm^2 after 90 min of irradiation at 17 mW/cm^2 at a 1/2 MIC concentration. Similarly, the blue OLED condition with an emitting area of 100 mm^2 began to exhibit antibacterial effects at an energy dose of 30.6 J/cm^2 after 30 min of irradiation at 17 mW/cm^2. Antibacterial activity was also maintained under 1/4 MIC conditions with irradiation lasting more than 60 min, with clear effects occurring from 120 min of irradiation.

This implies that a larger light area provides a more uniform treatment effect, and the absolute amount of light reaching the treated area increases, thereby enhancing the effect. This study confirmed that uniform treatment with a blue OLED could be achieved in a real-life setting, achieving excellent results at lower intensities due to the superior quantity of light, in contrast to previous studies that used a point light source and a higher output LED.

In future studies, to address the issues caused by drying, we plan to incorporate natural phytochemical substances in the form of gel, paste, or essence rather than simply dissolving them in DMSO and DI water. Additionally, these formulations will be evaluated through animal testing to assess their efficacy and safety.

Electronic Supplementary Material: Supplementary material (including captions for additional antibacterial effect experiments and analysis (Tables S1 and S2, Figs. S1–S11); research into compounds and the molecular characteristics of SO. L. (Table S1); ITO sheet resistance information (Table S2); expanded absorption spectrums of SO. L. solutions (Fig. S1); absorption spectrum of SO. L.'s components (Fig. S2); molecular structure of compound of SO. L. (Fig. S3); additional electro-optical properties of blue OLEDs (Fig. S4); platform and emission image of a patchable blue OLED (Fig. S5); additional image of the cell irradiation jig (Fig. S6); images of optical properties after the antibacterial effect (Fig. S7); evaluation of light dose over lifespan (Fig. S8); organized results of the antibacterial activity effect by concentration differences of SO. L. (Fig. S9); additional antibacterial effect with varying irradiation energy of blue OLED using various natural phytochemical substances (Fig. S10); evaluation of SO. L. solution depending on drying (Fig. S11)) is available in the online version of this article at https://doi.org/10.26599/NR.2025.94907409.

Data availability

All data needed to support the conclusions in the paper are presented in the manuscript and the Electronic Supplementary Material. Additional data related to this paper may be requested from the corresponding author upon request.

Acknowledgements

This research was supported by the National Research Foundation of Korea (NRF) grant funded by the Korea government (MSIT, No. 2022R1F1A1065534). Also, this research was also funded by the grant of the Korea Health Technology R&D Project through the Korea Health Industry Development Institute (KHIDI), funded by the Ministry of Health & Welfare, Republic of Korea (No. HI22C0290).

Declaration of competing interest

All the contributing authors report no conflict of interests in this work.

Author contribution statement

Y. W. K.: Conceptualization, data quration, formal analysis, writing – original draft, writing – review & editing, visualization. J.-Y. J.: Data quration, formal analysis, writing – original draft, writing – review & editing. E.-S. C.: Resources, funding acquisition. S. J. K.: Resources, funding acquisition. J. H. K.: Investigation, formal analysis. Y.-J. H.: Data curation, validation, resources, project administration. Y. J.: Conceptualization, resources, supervision, investigation, project administration, writing – review & editing. All the authors have approved the final manuscript.

Informed consent

Not applicable.

Ethics statement

Not applicable.

Use of AI statement

None.

References

[1] von Nussbaum, F.; Brands, M.; Hinzen, B.; Weigand, S.; Häbich, D. Antibacterial natural products in medicinal chemistry-exodus or revival. *Angew. Chem., Int. Ed.* **2006**, *45*, 5072–5129.

[2] Rachakonda, S.; Cartee, L. Challenges in antimicrobial drug discovery and the potential of nucleoside antibiotics. *Curr. Med. Chem.* **2004**, *11*, 775–793.

[3] Walsh, C. *Antibiotics: Actions, Origins, Resistance*; ASM Press: Washington, 2003.

[4] Del Giudice, P. Skin infections caused by *Staphylococcus aureus*. *Acta Derm. Venereol.* **2020**, *100*, 208–215.

[5] Hatlen, T. J.; Miller, L. G. Staphylococcal skin and soft tissue infections. *Infect. Dis. Clin. North Am.* **2021**, *35*, 81–105.

[6] Nowicka, D.; Grywalska, E. *Staphylococcus aureus* and host immunity in recurrent furunculosis. *Dermatology* **2019**, *235*, 295–305.

[7] Centers for Disease Control and Prevention (CDC). Four pediatric deaths from community-acquired methicillin-resistant *Staphylococcus aureus*—Minnesota and North Dakota, 1997–1999. *Arch Dermatol.* **1999**, *135*, 1566–1568.

[8] Hussain, F. M.; Boyle-Vavra, S.; Bethel, C. D.; Daum, R. S. Current trends in community-acquired methicillin-resistant *Staphylococcus aureus* at a tertiary care pediatric facility. *Pediatr. Infect. Dis. J.* **2000**, *19*, 1163–1166.

[9] Enright, M. C.; Robinson, D. A.; Randle, G.; Feil, E. J.; Grundmann, H.; Spratt, B. G. The evolutionary history of methicillin-resistant *Staphylococcus aureus* (MRSA). *Proc. Natl. Acad. Sci. USA* **2002**, *99*, 7687–7692.

[10] Scott, P.; Deye, G.; Srinivasan, A.; Murray, C.; Moran, K.; Hulten, E.; Fishbain, J.; Craft, D.; Riddell, S.; Lindler, L. et al. An outbreak of multidrug-resistant *Acinetobacter baumannii*-calcoaceticus complex infection in the US military health care system associated with military operations in iraq. *Clin. Infect. Dis.* **2007**, *44*, 1577–1584.

[11] Lu, M.; Dai, T. H.; Murray, C. K.; Wu, M. X. Bactericidal property of oregano oil against multidrug-resistant clinical isolates. *Front. Microbiol.* **2018**, *9*, 2329.

[12] Lu, M.; Wong, K. I.; Li, X.; Wang, F.; Wei, L.; Wang, S.; Wu, M. X. Oregano oil and harmless blue light to synergistically inactivate multidrug-resistant *Pseudomonas aeruginosa*. *Front. Microbiol.* **2022**, *13*, 810746.

[13] Wang, S.; Liu, X. Q.; Kang, O. H.; Kwon, D. Y. Combination of sanguisorbigenin and conventional antibiotic therapy for methicillin-resistant *Staphylococcus aureus*: Inhibition of biofilm formation and alteration of cell membrane permeability. *Int. J. Mol. Sci.* **2022**, *23*, 4232.

[14] Song, M. R.; Liu, Y.; Li, T. T.; Liu, X. J.; Hao, Z. H.; Ding, S. Y.; Panichayupakaranant, P.; Zhu, K.; Shen, J. Z. Plant natural flavonoids against multidrug resistant pathogens. *Adv. Sci.* **2021**, *8*, 2100749.

[15] Dai, J. K.; Han, R.; Xu, Y. J.; Li, N.; Wang, J. R.; Dan, W. J. Recent progress of antibacterial natural products: Future antibiotics candidates. *Bioorg. Chem.* **2020**, *101*, 103922.

[16] Li, M. C.; Sun, W. S.; Cheng, W.; Liu, D.; Liang, H.; Zhang, Q. Y.; Lin, W. H. Four new minor brominated indole related alkaloids with antibacterial activities from *Laurencia similis*. *Bioorg. Med. Chem. Lett.* **2016**, *26*, 3590–3593.

[17] Coppo, E.; Marchese, A. Antibacterial activity of polyphenols. *Curr. Pharm. Biotechnol.* **2014**, *15*, 380–390.

[18] Sasaki, H.; Matsumoto, M.; Tanaka, T.; Maeda, M.; Nakai, M.; Hamada, S.; Ooshima, T. Antibacterial activity of polyphenol components in oolong tea extract against *Streptococcus mutans*. *Caries Res.* **2004**, *38*, 2–8.

[19] Cao, J. H.; Han, J.; Xiao, H.; Qiao, J. P.; Han, M. Effect of tea polyphenol compounds on anticancer drugs in terms of anti-tumor activity, toxicology, and pharmacokinetics. *Nutrients* **2016**, *8*, 762.

[20] Yahfoufi, N.; Alsadi, N.; Jambi, M.; Matar, C. The immunomodulatory and anti-inflammatory role of polyphenols. *Nutrients* **2018**, *10*, 1618.

[21] Ibrahim, N. A.; Gouda, M.; Husseiny, S. M.; El-Gamal, A. R.; Mahrous, F. UV-protecting and antibacterial finishing of cotton knits. *J. Appl. Polym. Sci.* **2009**, *112*, 3589–3596.

[22] Wegener, M.; Hansen, M. J.; Driessen, A. J. M.; Szymanski, W.; Feringa, B. L. Photocontrol of antibacterial activity: Shifting from UV to red light activation. *J. Am. Chem. Soc.* **2017**, *139*, 17979–17986.

[23] Mohania, D.; Chandel, S.; Kumar, P.; Verma, V.; Digvijay, K.; Tripathi, D.; Choudhury, K.; Mitten, S. K.; Shah, D. Ultraviolet radiations: Skin defense–damage mechanism. In *Ultraviolet Light in Human Health, Diseases and Environment*. Ahmad, S. I., Ed.; Springer: Cham, 2017; pp 71–87.

[24] Pronin, S.; Koh, C. H.; Hughes, M. Cytotoxicity of ultraviolet-C radiation on a heterogeneous population of human glioblastoma multiforme cells: Meta-analysis. *Photodiagnosis Photodyn. Ther.* **2018**, *24*, 158–163.

[25] Matsumura, Y.; Ananthaswamy, H. N. Toxic effects of ultraviolet radiation on the skin. *Toxicol. Appl. Pharmacol.* **2004**, *195*, 298–308.

[26] Leelanarathiwat, K.; Katsuta, Y.; Katsuragi, H.; Watanabe, F. Antibacterial activity of blue high-power light-emitting diode-activated flavin mononucleotide against *Staphylococcus aureus* biofilm on a sandblasted and etched surface. *Photodiagnosis Photodyn. Ther.* **2020**, *31*, 101855.

[27] Lian, C.; Piksa, M.; Yoshida, K.; Persheyev, S.; Pawlik, K. J.; Matczyszyn, K.; Samuel, I. D. W. Flexible organic light-emitting diodes for antimicrobial photodynamic therapy. *npj Flex. Electron.* **2019**, *3*, 18.

[28] Paolillo, F. R.; Rodrigues, P. G. S.; Bagnato, V. S.; Alves, F.; Pires, L.; Corazza, A. V. The effect of combined curcumin-mediated photodynamic therapy and artificial skin on *Staphylococcus aureus*-infected wounds in rats. *Lasers Med. Sci.* **2021**, *36*, 1219–1226.

[29] Correia, J. H.; Rodrigues, J. A.; Pimenta, S.; Dong, T.; Yang, Z. C. Photodynamic therapy review: Principles, photosensitizers, applications, and future directions. *Pharmaceutics* **2021**, *13*, 1332.

[30] do Prado-Silva, L.; Brancini, G. T. P.; Braga, G. Ú. L.; Liao, X. Y.; Ding, T.; Sant'Ana, A. S. Antimicrobial photodynamic treatment (aPDT) as an innovative technology to control spoilage and pathogenic microorganisms in agri-food products: An updated review. *Food Control* **2022**, *132*, 108527.

[31] Jeon, Y.; Noh, I.; Seo, Y. C.; Han, J. H.; Park, Y.; Cho, E. H.; Choi, K. C. Parallel-stacked flexible organic light-emitting diodes for wearable photodynamic therapeutics and color-tunable optoelectronics. *ACS Nano* **2020**, *14*, 15688–15699.

[32] Jeon, Y.; Choi, H. R.; Kwon, J. H.; Choi, S.; Nam, K. M.; Park, K. C.; Choi, K. C. Sandwich-structure transferable free-form OLEDs for wearable and disposable skin wound photomedicine. *Light Sci. Appl.* **2019**, *8*, 114.

[33] Jeon, Y.; Choi, H. R.; Lim, M.; Choi, S.; Kim, H.; Kwon, J. H.; Park, K. C.; Choi, K. C. A wearable photobiomodulation patch using a flexible red-wavelength OLED and its *in vitro* differential cell proliferation effects. *Adv. Mater. Technol.* **2018**, *3*, 1700391.

[34] Piksa, M.; Fortuna, W.; Lian, C.; Gacka, M.; Samuel, I. D. W.; Matczyszyn, K.; Pawlik, K. J. Treatment of antibiotic-resistant bacteria colonizing diabetic foot ulcers by OLED induced antimicrobial photodynamic therapy. *Sci. Rep.* **2023**, *13*, 14087.

[35] Farivar, S.; Malekshahabi, T.; Shiari, R. Biological effects of low level laser therapy. *J. Lasers Med. Sci.* **2014**, *5*, 58–62.

[36] Smith, K. C. Laser (and LED) therapy is phototherapy. *Photomed. Laser Surg.* **2005**, *23*, 78–80.

[37] de Abreu Chaves, M. E.; de Araújo, A. R.; Piancastelli, A. C. C.; Pinotti, M. Effects of low-power light therapy on wound healing: LASER x LED. *An. Bras. Dermatol.* **2014**, *89*, 616–623.

[38] Choi, S.; Kwon, S.; Kim, H.; Kim, W.; Kwon, J. H.; Lim, M. S.; Lee, H. S.; Choi, K. C. Highly flexible and efficient fabric-based organic light-emitting devices for clothing-shaped wearable displays. *Sci. Rep.* **2017**, *7*, 6424.

[39] Song, H.; Song, Y. J.; Hong, J.; Kang, K. S.; Yu, S.; Cho, H. E.; Kim, J. H.; Lee, S. M. Water stable and matrix addressable OLED fiber textiles for wearable displays with large emission area. *npj Flex. Electron.* **2022**, *6*, 66.

[40] Ha, D.; Fang, Z. Q.; Zhitenev, N. B. Paper in electronic and optoelectronic devices. *Adv. Electron. Mater.* **2018**, *4*, 1700593.
[41] Guo, H. W.; Lin, L. T.; Chen, P. H.; Ho, M. H.; Huang, W. T.; Lee, Y. J.; Chiou, S. H.; Hsieh, Y. S.; Dong, C. Y.; Wang, H. W. Low-fluence rate, long duration photodynamic therapy in glioma mouse model using organic light-emitting diode (OLED). *Photodiagnosis Photodyn. Ther.* **2015**, *12*, 504–510.
[42] Triana, M. A.; Restrepo, A. A.; Lanzafame, R. J.; Palomaki, P.; Dong, Y. J. Quantum dot light-emitting diodes as light sources in photomedicine: Photodynamic therapy and photobiomodulation. *J. Phys.: Mater.* **2020**, *3*, 032002.
[43] Chen, H.; He, J.; Lanzafame, R.; Stadler, I.; Hamidi, H. E.; Liu, H.; Celli, J.; Hamblin, M. R.; Huang, Y. Y.; Oakley, E. et al. Quantum dot light emitting devices for photomedical applications. *J. Soc. Inf. Disp.* **2017**, *25*, 177–184.
[44] Lee, S. M.; Kim, S. H.; Kim, Z.; Lee, J. B. Photodynamic effects of topical photosensitizer, photodithazine using micro-LED for acne bacteria induced inflammation. *Ann. Dermatol.* **2024**, *36*, 329–340.
[45] Choi, J.; Lee, I. S.; Lee, J. S.; Jeon, S.; Yun, W. S.; Yang, S.; Moon, Y.; Kim, J.; Kim, J.; Choy, S. et al. Implantable micro-scale LED device guided photodynamic therapy to potentiate antitumor immunity with mild visible light. *Biomater. Res.* **2022**, *26*, 56.
[46] Jiang, W. Q.; Liang, M. K.; Lei, Q. F.; Li, G. Z.; Wu, S. The current status of photodynamic therapy in cancer treatment. *Cancers* **2023**, *15*, 585.
[47] Jeong, J. Y.; Hwang, Y. J. Natural phytochemical and visible light at different wavelengths show synergistic antibacterial activity against *Staphylococcus aureus*. *Pharmaceutics* **2024**, *16*, 612.
[48] Won, B. Y.; Shin, K. Y.; Ha, H. J.; Yun, Y. S.; Kim, Y. R.; Lee, H. G. Changes in nutritional composition of dropwort (*Oenanthe javanica*) ethanol extracts. *J. Korean Soc. Food Sci. Nutr.* **2015**, *44*, 882–887.
[49] Kim, S. G.; Kim, H. Y.; Kang, S. M. The effect of apple powder on quality characteristics and antioxidants in fried chicken breast. *Resour. Sci. Res.* **2023**, *5*, 50–60.
[50] Hmamou, A.; Eloutassi, N.; Alshawwa, S. Z.; Al Kamaly, O.; Kara, M.; Bendaoud, A.; El-Assri, E. M.; Tlemcani, S.; El Khomsi, M.; Lahkimi, A. Total phenolic content and antioxidant and antimicrobial activities of *Papaver rhoeas* L. organ extracts growing in taounate region, morocco. *Molecules* **2022**, *27*, 854.
[51] Jeong, J. Y.; Jung, I. G.; Yum, S. H.; Hwang, Y. J. *In vitro* synergistic inhibitory effects of plant extract combinations on bacterial growth of methicillin-resistant *Staphylococcus aureus*. *Pharmaceuticals* **2023**, *16*, 1491.
[52] Gupta, A.; Rosenberger, S. F.; Bowden, G. T. Increased ROS levels contribute to elevated transcription factor and MAP kinase activities in malignantly progressed mouse keratinocyte cell lines. *Carcinogenesis* **1999**, *20*, 2063–2073.
[53] Tocai, A. C.; Ranga, F.; Teodorescu, A. G.; Pallag, A.; Vlad, A. M.; Bandici, L.; Vicas, S. I. Evaluation of polyphenolic composition and antimicrobial properties of *Sanguisorba officinalis* L. and *Sanguisorba minor* Scop. *Plants* **2022**, *11*, 3561.
[54] Su, X. D.; Guo, R. H.; Yang, S. Y.; Kim, Y. H.; Kim, Y. R. Antibacterial effects of components from *Sanguisorba officinalis* L. on *Vibrio vulnificus* and their soluble epoxide hydrolase inhibitory activity. *Nat. Prod. Res.* **2019**, *33*, 3445–3449.
[55] Kim, S.; Oh, S.; Noh, H. B.; Ji, S.; Lee, S. H.; Koo, J. M.; Choi, C. W.; Jhun, H. P. *In vitro* antioxidant and anti-*Propionibacterium acnes* activities of cold water, hot water, and methanol extracts, and their respective ethyl acetate fractions, from *Sanguisorba officinalis* L. *roots*. *Molecules* **2018**, *23*, 3001.
[56] Sinsinwar, S.; Vadivel, V. Catechin isolated from cashew nut shell exhibits antibacterial activity against clinical isolates of MRSA through ROS-mediated oxidative stress. *Appl. Microbiol. Biotechnol.* **2020**, *104*, 8279–8297.
[57] Kurnia, D.; Ramadhanty, Z. F.; Ardani, A. M.; Zainuddin, A.; Dharsono, H. D. A.; Satari, M. H. Bio-mechanism of catechin as pheromone signal inhibitor: Prediction of antibacterial agent action mode by *in vitro* and *in silico* study. *Molecules* **2021**, *26*, 6381.
[58] Miklasińska, M.; Kępa, M.; Wojtyczka, R. D.; Idzik, D.; Dziedzic, A.; Wąsik, T. J. Catechin hydrate augments the antibacterial action of selected antibiotics against *Staphylococcus aureus* clinical strains. *Molecules* **2016**, *21*, 244.
[59] Gomes, F. M. S.; da Cunha Xavier, J.; dos Santos, J. F. S.; de Matos, Y. M. L.; Tintino, S. R.; de Freitas, T. S.; Coutinho, H. D. M. Evaluation of antibacterial and modifying action of catechin antibiotics in resistant strains. *Microb. Pathog.* **2018**, *115*, 175–178.
[60] Renzetti, A.; Betts, J. W.; Fukumoto, K.; Rutherford, R. N. Antibacterial green tea catechins from a molecular perspective: Mechanisms of action and structure–activity relationships. *Food Funct.* **2020**, *11*, 9370–9396.
[61] Cota, D.; Patil, D. Antibacterial potential of ellagic acid and gallic acid against IBD bacterial isolates and cytotoxicity against colorectal cancer. *Nat. Prod. Res.* **2023**, *37*, 1998–2002.
[62] Macêdo, N. S.; Dos Santos Barbosa, C. R.; Bezerra, A. H.; de Sousa Silveira, Z.; da Silva, L.; Coutinho, H. D. M.; Dashti, S.; Kim, B.; da Cunha, F. A. B.; da Silva, M. V. Evaluation of ellagic acid and gallic acid as efflux pump inhibitors in strains of *Staphylococcus aureus*. *Biol. Open* **2022**, *11*, bio059434.
[63] Tian, Q. M.; Wei, S. M.; Su, H. R.; Zheng, S. M.; Xu, S. Y.; Liu, M. J.; Bo, R. N.; Li, J. G. Bactericidal activity of gallic acid against multi-drug resistance *Escherichia coli*. *Microb. Pathog.* **2022**, *173*, 105824.
[64] Kiran, K.; Patil, K. N. Gallic acid inhibits *Staphylococcus aureus* RecA protein functions: Role in countering antibiotic resistance in bacteria. *J. Appl. Microbiol.* **2024**, *135*, lxad227.
[65] Qi, W. D.; Qi, W. X.; Xiong, D. W.; Long, M. Quercetin: Its antioxidant mechanism, antibacterial properties and potential application in prevention and control of toxipathy. *Molecules* **2022**, *27*, 6545.
[66] Nguyen, T. L. A.; Bhattacharya, D. Antimicrobial activity of quercetin: An approach to its mechanistic principle. *Molecules* **2022**, *27*, 2494.
[67] Aguilera-Correa, J. J.; Fernández-López, S.; Cuñas-Figueroa, I. D.; Pérez-Rial, S.; Alakomi, H. L.; Nohynek, L.; Oksman-Caldentey, K. M.; Salminen, J. P.; Esteban, J.; Cuadros, J. et al. Sanguiin H-6 fractionated from cloudberry (*Rubus chamaemorus*) seeds can prevent the methicillin-resistant *Staphylococcus aureus* biofilm development during wound infection. *Antibiotics* **2021**, *10*, 1481.
[68] Gesek, J.; Jakimiuk, K.; Atanasov, A. G.; Tomczyk, M. Sanguiins-promising molecules with broad biological potential. *Int. J. Mol. Sci.* **2021**, *22*, 12972.
[69] Wang, X. Y.; Wang, L.; Fekrazad, R.; Zhang, L.; Jiang, X.; He, G.; Wen, X. Polyphenolic natural products as photosensitizers for antimicrobial photodynamic therapy: Recent advances and future prospects. *Front. Immunol.* **2023**, *14*, 1275859.
[70] Abrahamse, H.; Hamblin, M. R. New photosensitizers for photodynamic therapy. *Biochem. J.* **2016**, *473*, 347–364.
[71] Sarker, M. A. R.; Ahn, Y. H. Photodynamic inactivation of multidrug-resistant bacteria in wastewater effluent using green phytochemicals as a natural photosensitizer. *Environ. Pollut.* **2022**, *311*, 120015.
[72] Sarker, M. A. R.; Ahn, Y. H. Green phytoextracts as natural photosensitizers in LED-based photodynamic disinfection of multidrug-resistant bacteria in wastewater effluent. *Chemosphere* **2022**, *297*, 134157.
[73] dos Santos, D. P.; Galantini, M. P. L.; Ribeiro, I. S.; Muniz, I. P. R.; Pereira, I. S.; da Silva, R. A. A. Photoactivated resveratrol controls intradermal infection by *Staphylococcus aureus* in mice: A pilot study. *Lasers Med. Sci.* **2020**, *35*, 1341–1347.
[74] Despa, F.; Orgill, D. P.; Neuwalder, J.; Lee, R. C. The relative thermal stability of tissue macromolecules and cellular structure in burn injury. *Burns* **2005**, *31*, 568–577.

This is an open access article under the terms of the Creative Commons Attribution 4.0 International License (CC BY 4.0, https://creativecommons.org/licenses/by/4.0/).

© The Author(s) 2025. Published by Tsinghua University Press.